Strain-Induced Phenomena in Amorphous and Semicrystalline Elastomers. Solid State ^{1}H NMR T_2 Relaxation under Uniaxial Compression

V. M. Litvinov

DSM Research, P.O.Box 18, 6160 MD Geleen, The Netherlands

Received February 5, 2001; Revised Manuscript Received July 15, 2001

ABSTRACT: The strain-induced phenomena in cured amorphous EPDM and semicrystalline ethane−octene copolymer (*m*-PE) were studied using ^{1}H T_2 NMR relaxation. Samples studied differed with regard to network structure; i.e., EPDM had a larger density of chemical cross-links, whereas the total network density in *m*-PE was significantly larger because of chain anchoring to crystallites. The effect of these differences on elastic properties was compared. A compression unit was developed for these experiments. This device made it possible to perform NMR experiments under fixed uniaxial compression and to record applied force. Despite the larger total network density in *m*-PE, the orientation of elastic chains under compression in EPDM is significantly greater, suggesting that the density of chemical cross-links largely determines the elastic behavior. It appears that crystallites in *m*-PE rearrange upon compression without a change in the crystallinity. It can be concluded from this study that an increase in the density of chemical cross-links is required to improve the compression set of *m*-PE.

1. Introduction

Large and reversible elastic deformation is one of the most important characteristics of natural and synthetic rubbers. The configuration of polymer chains changes upon applied stress from a coiled to an extended one, causing retractive force. Uniaxial extension and compression are the most common tests used to characterize the mechanical properties of rubbery materials and the density of network junctions. Large recovery of rubbery materials after the removal of compression force, i.e., low compression set, is usually required for many applications of rubbery materials. Statistical rubber elasticity theories established the stress-strain relationship for "ideal" polymer networks, i.e., networks with a homogeneous distribution of network junctions and a narrow distribution of the length of network chains.[1,2] However, there is still a considerable debate about the validity and applicability of these theories for heterogeneous networks and on the effect of physical network junctions and network defects on viscoelasticity. The interpretation of the mechanical properties is even more uncertain for heterogeneous rubbery material, such as filled rubbers, rubbery blends, block copolymers, and rubbery materials exhibiting crystallinity. It is difficult to determine the effects of these heterogeneities on mechanical properties using techniques that measure macroscopic, volume-average properties. Physical methods that provide information on the molecular level are the most suitable for determining the response of heterogeneous structures to macroscopic deformation. This knowledge is desired for a better understanding of the mechanical properties of heterogeneous rubbery materials.

Proton spin−spin relaxation (T_2) NMR relaxation is one of the methods which have been used for analysis of strain-induced chain elongation in uniaxially stretched rubbery materials.[3−8] These studies show that the method provides information about chain elongation under strain,[3−8] strain-induced crystallization,[4] and the effect of deformation on rigid domains in elastomeric block copolymers.[5] In these studies, constant strain was maintained during NMR experiments using a mechanical holder or an adhesive. The effect of stress relaxation during sample preparation and NMR experiments cannot be evaluated in these experiments. NMR experiments under uniaxial compression are less demanding as regards sample preparation. Although analysis of experimental data with respect to strain-induced chain elongation is more complicated than that for uniaxial extension, the applied force can be measured as a function of time.

Phase composition in semicrystalline polymers and its changes upon deformation have been often studied by proton T_2 relaxation. The polymer most frequently studied using this method is poly(ethylene) (PE).[9−17] In general, the results of these experiments suggest a three-phase model. According to these experiments, PE samples are composed of a crystalline phase, a semirigid phase and a soft amorphous phase. Relative fractions of polymer chains in crystalline, intermediate and soft amorphous phases can be determined using this method. A good correlation was observed between crystallinity measured by NMR and that measured by other methods. Molecular mobility and chain conformation in the interphase are intermediate between the rigid all-*trans* crystalline phase and soft *trans*−*gauche* amorphous phase.[18−22] It was noted that the fraction of the intermediate phase depends on the technique, the temperature and the method of data evaluation. In many respects, the intermediate phase has a kinetic origin and may not be considered as a true thermodynamical phase. Apparently, the definition *an interface* or *a semirigid fraction of the amorphous phase* is more appropriate for the third phase. Distinct differences in chain mobility in different PE phases are apparently caused by a short statistical segment of poly(ethylene) chain, which is about seven carbon−carbon bonds.[23] This results in a rapid loss of configurational entropy and restrictions on rotational and translational chain mobility when moving away from the crystalline phase.

10.1021/ma010208k CCC: $20.00
Published on Web 10/18/2001

In this study, a compression unit was developed for proton relaxation experiments under constant uniaxial compression. The unit measures applied force and makes it possible to perform NMR experiments at different compressions and temperatures. The method was used to study strain-induced phenomena in two cross-linked elastomers, i.e., amorphous EPDM and semicrystalline ethylene−octene copolymer (*m*-PE). The effect on the strain-induced elongation of chains between chemical cross-links and physical junctions that originate from the crystalline phase was studied.

2. Experimental Section

2.1. Sample Preparation and Characterization. Ethylene/1-octene copolymer (*m*-PE) was prepared with a metallocene catalyst and contained 30 mass % octene chain units. The specific density of the initial sample was 0.882 g/cm^3. EPDM was composed of 55.5, 40, and 4.5 mass % ethylene, propylene, and dicyclopentadiene chain units, respectively. Both samples were cured with 7.4 mass % Perkadox 14/40, which consisted of 40 mass % bis(*tert*-butylperoxyisopropyl)benzene in PP powder. Perkadox 14/40 was mixed with polymers in a batch kneader using screw rotation of 60 turns per min. Mixing time was 5 min and the temperature of the melt was 130 °C. The temperature rose during mixing to 135 and 141 °C for *m*-PE and EPDM, respectively. Since no increase in torque was observed during kneading, this suggests that temperatures were low enough to avoid pre-cross-linking. Samples were cured for 10 min at 180 °C in a mold consisting of several cylindrical holes of 4.4 mm in diameter. The mold thickness was 4 mm. After curing, the pressure in the mold was removed at 100 °C.

2.2. ^{1}H Solid-State NMR Measurements and Data Analysis. Proton low resolution NMR T_2 relaxation experiments were performed on a Bruker Minispec NMS-120 spectrometer for nonspinning samples. This spectrometer operates at a proton resonance frequency of 20 MHz. The length of the 90° pulse and the dead time were 2.8 and 7 μs, respectively. A BVT-3000 temperature controller was used for temperature regulation. The temperature gradient and stability were better than 1 °C.

Several precautions have to be taken to accurately measure the transverse magnetization decay for (micro) heterogeneous materials containing both low mobile and highly mobile fractions. *The errors cannot practically be eliminated, but their effects can be minimized to a large extent.* Two different pulse sequences were used to record the decay of the transverse magnetization (T_2 decay) from both (semi-)rigid and mobile fractions of the samples as described previously. *The solid-echo pulse sequence* (SEPS), $90°_x - t_{se} - 90°_y - t_{se} -$ [acquisition: $A(\tau)$], with $t_{se} = 10$ μs was used to determine *the T_2 relaxation time and the proton content of the (semi-)rigid fraction of the samples*. The time after the first pulse $\tau = (2t_{se} + t_{90}/2)$, where t_{90} is the duration of the 90° pulse, was taken as zero. *The Hahn-echo pulse sequence* (HEPS), $90°_x - t_{He} - 180°_x - t_{He} -$ (acquisition), was used to record t*he slow decay for the mobile fraction of the samples*. The second pulse in the HEPS inverts nuclear spins of mobile molecules only and an echo signal is formed with a maximum $A(\tau)$ at time $\tau = (2t_{He} + t_{180}/2)$ after the first pulse, where t_{180} is the duration of the 180° pulse. By varying the pulse spacing in the HEPS, the amplitude of the transverse magnetization, $A(\tau)$, is measured as a function of time τ. The HEPS makes it possible to eliminate the magnetic field and chemical shift inhomogeneities, and to accurately measure the T_2 relaxation time for mobile materials.

The time constants (T_2 relaxation time) that are characteristic of different slopes in the magnetization decay curve were obtained by performing a least-squares fit of the data using a linear combination of Weibull and exponential functions for analysis of the T_2 decay, as measured using the SEPS:

$$A(\tau) = A(0)^s \exp[-(\tau/T_2{}^s)^\alpha] + A(0)^l \exp[-(\tau/T_2{}^l)] \quad (1)$$

where $A(0)^{s,l}$ is the fractional amplitude of the relaxation components, $T_2{}^{s,l}$ is the characteristic decay time, and α is the decay shape parameter that might be related to the distribution of the relaxation time. *The relative fraction of the relaxation components*, $A(0)^s/[A(0)^s + A(0)^l]$ and $A(0)^l/[A(0)^s + A(0)^l]$, as designated in the text by % $T_2{}^s$ and % $T_2{}^l$, represents the fraction of hydrogen in phases/components with different molecular mobilities. It is noted that the analysis of T_2 decays from heterogeneous materials is far from straightforward. The Weibull function is often used in describing T_2 relaxation of heterogeneous rigid solids. T_2 relaxation of highly mobile materials can be often described by exponential function. Only the initial part of the decay ($0 = \tau < 400$ μs), which was measured using the SEPS, was fitted. In this fit, the baseline was fixed to the value that was measured at the same conditions after the sample was removed from the NMR probe. The baseline position, as determined in this way, coincided within 1% with its value that was obtained from the least-squares analysis of the T_2 decay measured using the HEPS. An exponential function was used for analysis of the T_2 decay, as measured using the HEPS.

The error in the relaxation parameters is composed of (a) experimental errors (about 2%), (b) an error caused by a chosen fitting function (estimated to be about 5%), and (c) uncertainties regarding the fitting (about 0.5%). Repeated experiments for the same sample indicate that the reproducibility of the results was higher than 2−3%.

The T_2 relaxation experiments were performed at heating samples from room temperature to 120°C. Then the samples were cooled to room temperature at a rate of about 20°/min and the measurements were performed by subsequently cooling samples to −50 °C. The NMR experiments at each temperature took about 25 min.

2.3. Calculation of the Mean Molar Mass of Network Chains. The distinguishing feature of T_2 relaxation for viscoelastic networks is the high-temperature plateau that is observed at temperatures well above T_g. The temperature independence of T_2 is attributed to constraints, which limit the number of possible conformations of a network chain with respect to those of a free chain. A value of T_2 at the plateau, $T_2{}^{pl}$, is determined by the asymmetry of random rotations of monomer units and does not depend on the mechanism and frequency of motions of network chains. The theory of the transverse relaxation in elastomeric networks relates $T_2{}^{pl}$ to the number of statistical segments, *Z*, between *c*hemical and *p*hysical network junctions:[24−26]

$$Z = (T_2{}^{pl})/[a(T_2{}^{rl})] \quad (2)$$

where *a* is the theoretical coefficient, which depends on the angle between the segment axis and the internuclear vector for the nearest nuclear spins at the main chains.[24,25] For polymers containing aliphatic protons in the main chain, the coefficient *a* is close to 6.2 ± 0.7.[25] It is noted that the *a* value is similar for EPDM and *m*-PE due to large similarity in the polymer backbone structure. $T_2{}^{rl}$ of 10.4 ± 0.4 μs is the relaxation time which is measured at −150 °C for the polymers swollen in 1,1,2,2- $C_2D_2Cl_4$.This temperature is far below T_g of *m*-PE and EPDM as well as of the solvent.

Using the number of backbone bonds in the statistical segment, C_∞, weight average molar mass of network chains between chemical and physical junctions, $\langle M_{c+p}\rangle_w$, is calculated:

$$\langle M_{c+p}\rangle_w = ZC_\infty M_u/n \quad (3)$$

where M_u is the *average* molar mass per two carbon−carbon backbone bonds ($n = 2$). The molar mass of hexyl groups is accounted for in a value of M_u for *m*-PE. C_∞ for EPDM and *m*-PE equals about 6.5−7 backbone bonds.[26,27] The maximum, relative error of this NMR network density determination is estimated to be about 15−25%.[26]

The quantitative determination of the network density in *m*-PE is complicated because of the presence of hexyl branches.

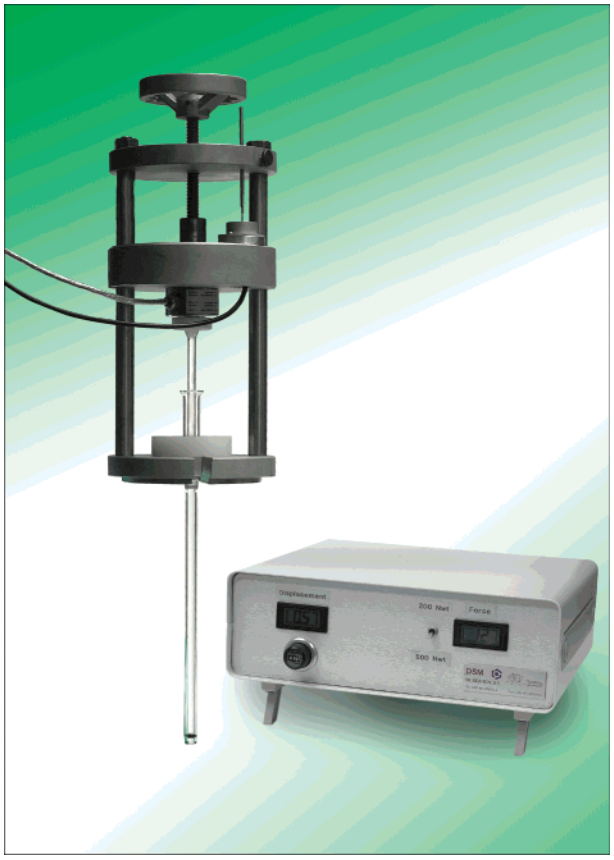

Figure 1. Picture of the compression unit.

It has been well established that the mobility of short side groups and chain-end blocks is somewhat higher than that of the main chain and that the mobility increases when moving toward the chain end. In a highly simplified approach, $(T_2)^{-1}$ is the weight average of the intrinsic relaxation rate of the backbone protons of network chains and that of the side chains:

$$(T_2)^{-1} = f_n(1/T_2^{net}) + (1 - f_n)(1/T_2^{sc}) \quad (4)$$

where f_n is the fraction of backbone protons and T_2^{net} and T_2^{sc} are the intrinsic relaxation times of network chains and side chains, respectively. The fraction of hexyl protons, $(1 - f_n)$, in the sample is about 27%. Since the shape of the T_2 relaxation decay for *m*-PE in the molten state is close to exponential, this suggests that the ratio $(T_2^{sc}:T_2^{net})$ is below 3 as a result of strong coupling in the mobility of main chain and side groups. According to eq 4, the side groups in this case provide a moderate contribution to the total relaxation rate (about 15%).

2.4. NMR under Compression. Proton T_2 relaxation experiments for the samples under uniaxial compression were performed using a home-built device (Figure 1). The sample disk has a diameter of 4.4 mm and a height, h_o, of 4 mm. The sample was placed in a glass tube that was fixed to a static frame assembled with a Minispec magnet. The sample compression was performed with a 6-mm diameter glass rod. The glass rod fitted tightly inside the glass tube. The glass rod was moved along the NMR tube using a screw. The sample compression was measured with a micrometer with an accuracy of 0.01 mm. The applied force was measured using a force meter with an accuracy of 1 N. The permanent magnetic field was perpendicular to the force direction. Precautions were taken to avoid sample tilting and constrained deformation due to contact between the sample and the walls of the tube. Uniaxial compression causes biaxial extension in the direction perpendicular to the applied force. It should be mentioned that strain distribution through the sample could strongly deviate from biaxial extension due to shear deformation which can be caused by the following reasons: (a) small sample *height: diameter* ratio, (b) adhesion of the sample to the glass surface, and (c) a curvature of the bottom of the glass tube and the bottom surface of the glass rod. Since the chain elongation differs for uniaxial compression and simple shear, i.e., it is proportional to $(\lambda^2 - 1/\lambda)$ and λ (where λ is a deformation ratio),[1,2] *no quantitative information* can be obtained on strain-induced chain orientation. In the present study, the method is used for determining *relative difference in chain elongation upon compression* with respect to the density of chemical cross-links and physical network junctions in EPDM and *m*-PE.

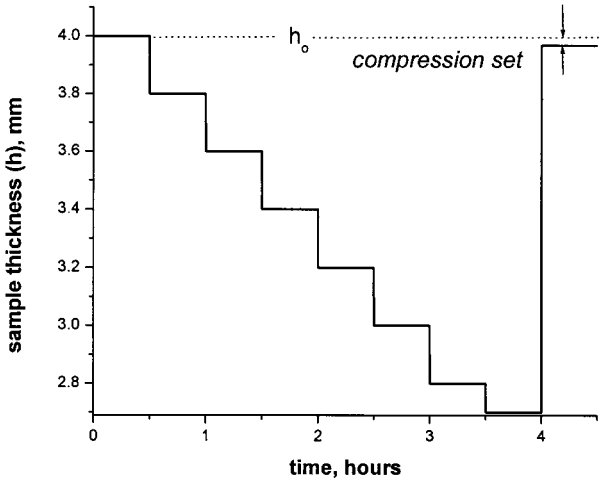

Figure 2. Displacement as a function of time during NMR experiments for EPDM at 27 °C. The measurements were performed after each subsequent change of the deformation. The sample reveals small residual strain (compression set) after the force was removed.

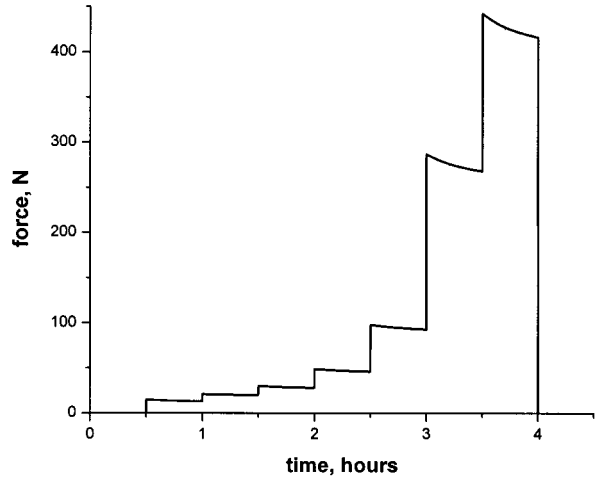

Figure 3. Force as a function of time during NMR T_2 relaxation experiments for EPDM at 27 °C.

3. Results and Discussion

3.1. Force as a Function of Deformation. ^{1}H T_2 relaxation experiments are performed on undeformed EPDM and *m*-PE, on the samples subjected to different compression and on samples shortly after the compression force was removed. A stepwise increase of the uniaxial compression is used in the present study. Deformation and compression force are shown in Figures 2−5. Stress relaxation causes about a 5% decrease in compression force during NMR experiments that take about 25 min. Cured EPDM demonstrates good elastic recovery, contrary to *m*-PE, which shows large residual strain after the force is removed, i.e., compression set. Compression force as a function of compression is

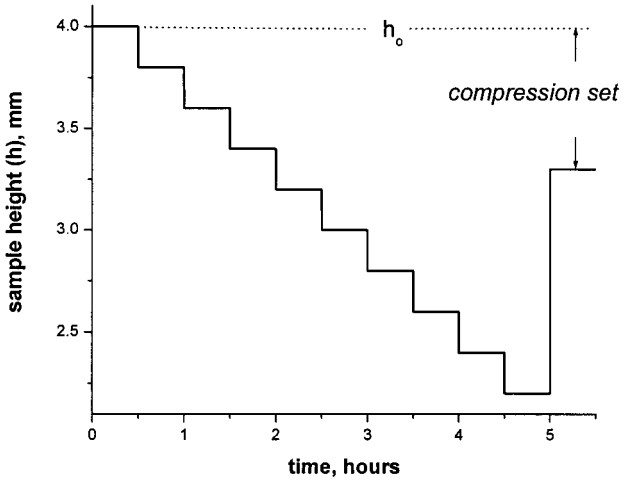

Figure 4. Displacement as a function of time during NMR experiments for *m*-PE at 27 °C. The measurements were performed after each subsequent change in deformation. The sample reveals large residual strain (compression set) after the force was removed.

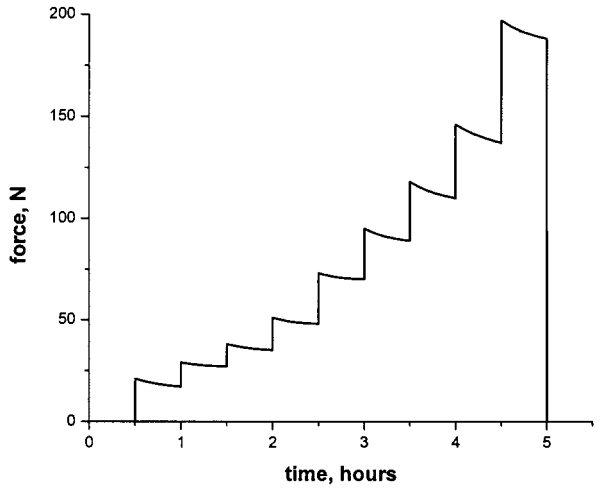

Figure 5. Force as a function of time during NMR T_2 relaxation experiments for *m*-PE at 27 °C.

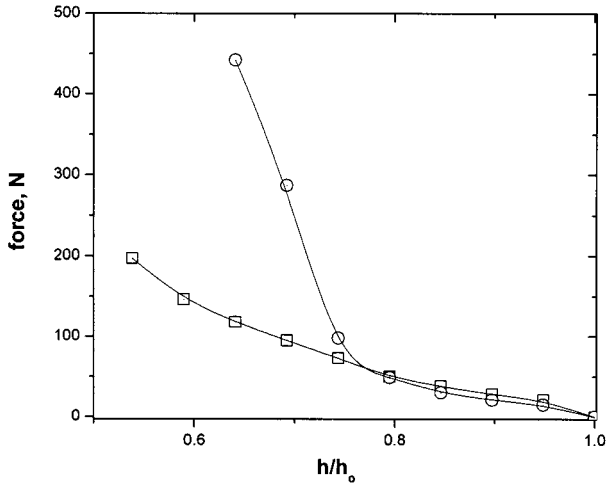

Figure 6. Compression force versus compression, h/h_o, for *m*-PE (squares) and EPDM (circles). h_o and h are the heights of the initial and compressed samples. The force was measured shortly after each subsequent increase in compression.

compared for EPDM and *m*-PE in Figure 6. Despite the same vulcanization procedure, the samples reveal large differences in stress−strain behavior at large deformations. Several factors could cause this difference: (a) a difference in the density of chemical cross-links, which will affect the finite chain extensibility; (b) strain-induced crystallization; (c) morphological changes in *m*-PE under deformation; (d) difference in stress relaxation of the samples. Mechanical tests alone do not allow determination of the effect of these factors for compression force. Proton NMR T_2 relaxation experiments are used below to determine the effect of compression on crystallinity and strain-induced chain elongation in the amorphous phase of *m*-PE compared to that of amorphous EPDM.

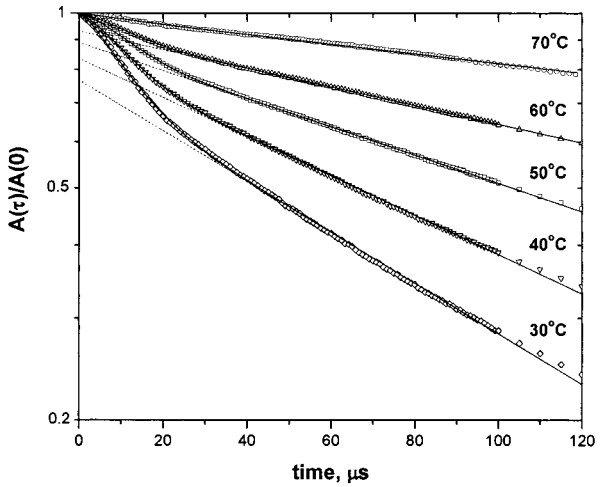

Figure 7. Decay of the transverse magnetization (points) at different temperatures for undeformed *m*-PE. The decay was measured using the SEPS. Solid lines represent the result of a least-squares adjustment of the decay with a linear combination of Weibull and exponential functions. Dotted lines show the relaxation component with long decay time. The experiments were performed at subsequent heating of the sample from room temperature to 70 °C.

3.2. Crystallinity and the Density of Chemical Cross-Links and Physical Junctions. Below 70 °C, the decay of the transverse magnetization for *m*-PE can be described by two distinct components (see eq 1 and Figure 7). One component has a **s**hort decay time, T_2^s, which is typical for crystalline and glassy materials. A value of T_2^l for the component with a **l**ong decay time is comparable to T_2 for amorphous EPDM. The relative fractions of the components for *m*-PE, % T_2^s and % T_2^l, correspond to the content of hydrogen in rigid and soft phases, respectively. It is noted that no statistically relevant analysis of the T_2 decay for *m*-PE can be obtained with a three-component model which is usually used for linear PE.[9−17] It might be suggested that (1) chain mobility at crystal-amorphous interface in *m*-PE is larger compared to that to that for linear PE because of small size of crystals and crystal imperfections and (2) broad distribution of the correlation time for chain motions exists in the amorphous phase which can cause "apparent" single-exponential relaxation.

The temperature dependence of the T_2 relaxation parameters for *m*-PE and EPDM is shown in Figures 8 and 9. Both T_2^s and T_2^l increase upon heating, which corresponds to an increase in the frequency and/or amplitude of chain motions in crystalline and amorphous phases, respectively. The large increase in the content of rigid material, % T_2^s, below 0 °C is apparently caused by immobilization of chain units adjacent to the crystalline phase as T_g of *m*-PE is approached. It should be noted that T_g at the time scale of the NMR experi-

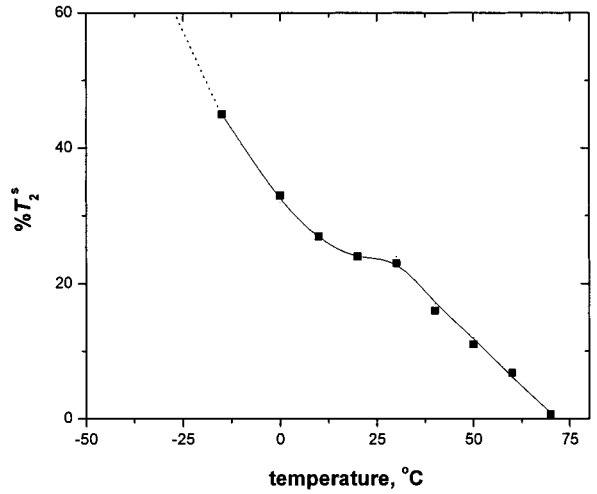

Figure 8. Temperature dependence of the content of rigid fraction for undeformed *m*-PE, % T_2^s. The experiments were performed at subsequent heating of the sample from room temperature to 70 °C and its cooling from room temperature to −60 °C (see part 2.2). % T_2^s was measured using the SEPS.

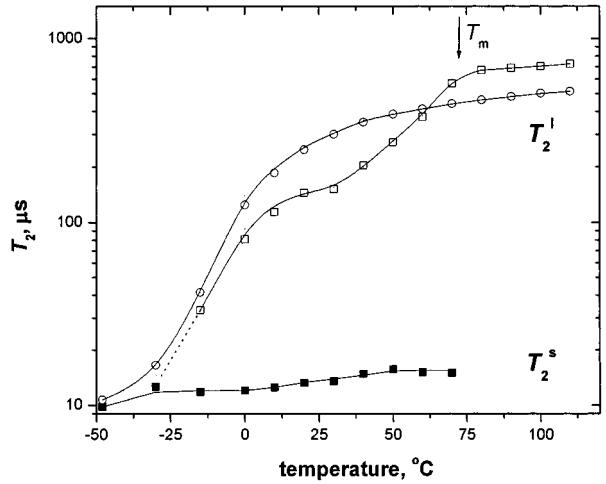

Figure 9. Temperature dependence of the T_2 relaxation time T_2^s and T_2^l for undeformed *m*-PE (squares) and T_2 for EPDM (circles). The experiments were performed at subsequent heating of the sample from room temperature to 120 °C and its cooling from room temperature to −60 °C (see part 2.2). Melting temperature, T_m, of the crystalline phase of *m*-PE is shown by an arrow. Values of T_2^s and T_2^l were measured with the SEPS and the HEPS, respectively.

ment is comparable with the glass transition, as measured by the dynamic mechanical experiment at a frequency of about 20 kHz. T_g^{NMR} is observed 30−50 °C above T_g, as measured by DSC. Above room temperature, % T_2^s decreases significantly with increasing temperature and approaches zero at 70 °C. This temperature corresponds to the peak of melting as measured by DSC. According to DSC, crystallinity of the sample also decreases gradually upon heating above 0 °C. Apparently, the change in % T_2^s at the temperatures indicated is caused mainly by a gradual decrease in crystallinity. It was noted that maximum crystallinity of *m*-PE and linear low-density PE, which have a specific density similar to that of the studied sample, equals about 20−30%.[28−30] The value of % T_2^s at room temperature is in the same range (see Figure 8). This strongly suggests that *T_2^s and T_2^l relaxation components originate from crystalline and amorphous phases in m-PE*, and % *T_2^s corresponds to the crystallinity*. It appears that the simple two-phase model is applicable for analysis of the T_2 relaxation data for *m*-PE.

Analysis of the temperature dependence of the T_2 relaxation for cured amorphous polymers makes it possible to determine the network structure.[24−26] The T_2 relaxation at temperatures well above T_g is related to the density of chemical cross-links and chain entanglements in vulcanizates.[24−26] The T_2^l relaxation time for the amorphous phase in semicrystalline polymers is determined largely by the mean length of amorphous chains between anchoring points to crystalline phase.[31] Moreover, the effect of confinement of amorphous segments by crystalline lamella induces an additional constrains of segmental motions in the amorphous phase.[32]

Above 80 °C, T_2 for EPDM and *m*-PE reaches nearly constant plateau value. At these temperatures, *m*-PE is amorphous and T_2 is determined for both samples by the density of chemical cross-links and chain entanglements. The estimated length of network chains (see part 2.3) equals 50 and 80 backbone carbon atoms of EPDM and *m*-PE chains, respectively. These values correspond to mean molar masses of network chains of 840 and 1900 g/mol, respectively. The molar mass of network chains is smaller than the entanglement density in these polymers.[23,26,27] Therefore, a large fraction of chain entanglements is trapped by chemical cross-links. Despite the same curing procedure, the density of chemical cross-links in *m*-PE is significantly smaller compared to that in EPDM for the following reason. It has been well established that hydrogen abstraction is more likely from tertiary carbon atoms than from secondary and primary ones. Peroxide curing of EPDM occurs by combination of two macroradicals, which are formed in olefinic chain portions, and by addition of the macroradicals to chain units bearing an unsaturation.[33] Since the molar fraction of tertiary carbons in *m*-PE is smaller by a factor of 2 compared to EPDM and EPDM contains additionally unsaturations, these results in low curing efficiency of *m*-PE.

Below 70 °C, a decrease in T_2^l for *m*-PE is significantly larger compared to that for EPDM. This is apparently caused by crystallization of *m*-PE. As a result of the small size of crystals in *m*-PE,[28−30] crystallites form numerous multifunctional physical network junctions. Below 60 °C, the total density of network junctions in *m*-PE is significantly larger compared to the density of chemical cross-links and chain entanglements in EPDM, as can be seen from values of T_2 (Figure 9).

3.3. Strain-Induced Phenomena in Compressed Elastomers. The T_2 decay for EPDM and *m*-PE at different compressions is shown in Figures 10 and 11. The crystallinity of *m*-PE is not affected by compression, as is shown by the results in Figure 11. The rate of T_2 relaxation for EPDM and the amorphous phase of *m*-PE increases upon compression, which is caused by strain-induced elongation of network chains. The effect of compression on the chain elongation is compared for *m*-PE and EPDM in Figure 12. The dependence of $1/T_2$ is plotted against $\lambda^2 - \lambda^{-1}$, where $\lambda = (h/h_o)^{-0.5}$. According to the classical theory of affine deformation of uncompressible samples, the segmental orientation of elastically effective network chains is proportional to the deformation function $\lambda^2 - \lambda^{-1}$ and scales with Z^{-1}, where Z is the number of statistical segments per network chains.[1,2,34] It should be noted that deformation mechanisms of *m*-PE is not fully understood because of

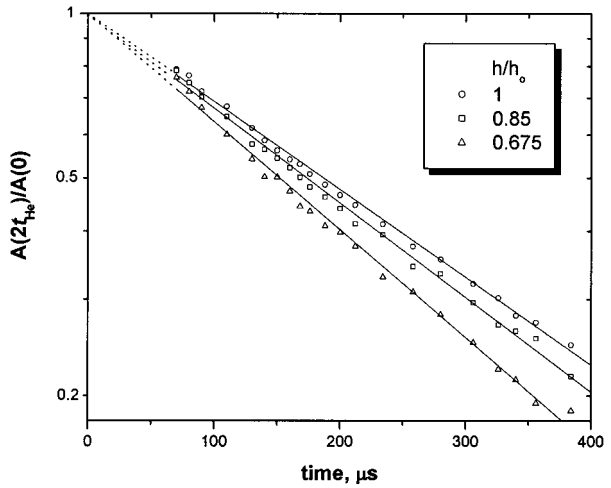

Figure 10. Decay of the transverse magnetization (points) for EPDM at 27 °C for different compression, h/h_o, where h_o and h are the heights of the initial and compressed samples. The decay was measured using the HEPS. Solid lines represent the result of a least-squares adjustment of the decay with an exponential function.

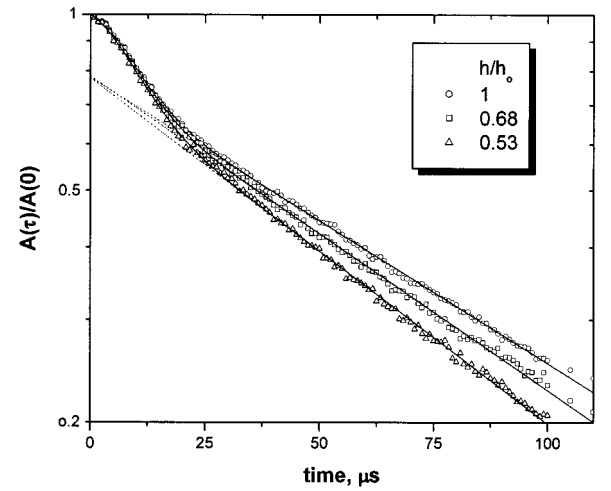

Figure 11. Decay of the transverse magnetization (points) for *m*-PE at 27 °C for different compression, h/h_o, where h_o and h are the height of the initial and compressed samples. The decay was measured using the SEPS. Solid lines represent the result of a least-squares adjustment of the decay with a linear combination of Weibull and exponential functions. Dotted lines show the relaxation component with long decay time.

complex morphology of these materials. At a specific density above 0.87 g/cm^3, a large fraction of crystalline phase is composed of lamella though granular structures are also present, which means that the chains crystallize into small, blocky crystallites.[28,35] Below this density, the morphology changes to granular based with a small fraction of lamella. Depending on the density and applied strain, viscoelastic and plastic deformation mechanisms could govern the stress−strain behavior of *m*-PE. Recent studies suggest that at moderate deformations the classical rubber elasticity theory can describes stress−strain behavior of *m*-PE with density below 0.888 g/cm^3.[36,37] However, the possibility of the plastic deformation of crystallites in the *m*-PE sample studied cannot be ruled out.

The current experiments provide relative differences in the chain elongation upon compression, as determined by the slope of the dependence $1/T_2$ against $\lambda^2 - \lambda^{-1}$. Since the experiments are performed at 27 °C, which is in vicinity of the high-temperature plateau (see Figure 9 and part 2.3), $1/T_2$ values are mainly determined by strain induced chain elongation and do not depend on a change in frequency of chain motions caused by deformation. Despite larger total density of network junctions in *m*-PE, the orientation of elastomeric chains for EPDM is larger by a factor of 2. This difference can be a result of the following. It has been shown that longitudinal diffusion of PE chains through the crystalline phase into the amorphous one occurs in linear PE.[38] The characteristic time constant of the diffusion process is proportional to the square of the crystalline thickness. As a result of imperfections and the small size of crystallites in *m*-PE,[28−30] one might suggest rather fast chain mobility in *m*-PE crystals. Chain diffusion along the chain direction can be restricted due to chain branches that are presumably excluded out of the crystalline phase.[39,40] However, overstrained chains can be detached from the crystal surface and a new crystal can be formed at another place, or chain(s) in the vicinity of the crystal surface can be attached to the crystal. Since crystallinity of *m*-PE remains constant, it might be suggested that the mean length of chain interconnecting neighboring crystals is not affected by crystal rearrangements and it is mainly determined by the chain microstructure. These rearrangements of crystallites can reduce chain elongation under compression. A recently performed stress−strain analysis of uniaxially stretched *m*-PE suggested also rearrangements of physical network junctions originating from crystallites.[36,41] Stress−strain curves can be well described by the slip−link theory of rubber elasticity, suggesting that chains attached to the crystal surface can slide along the chain contour.[36]

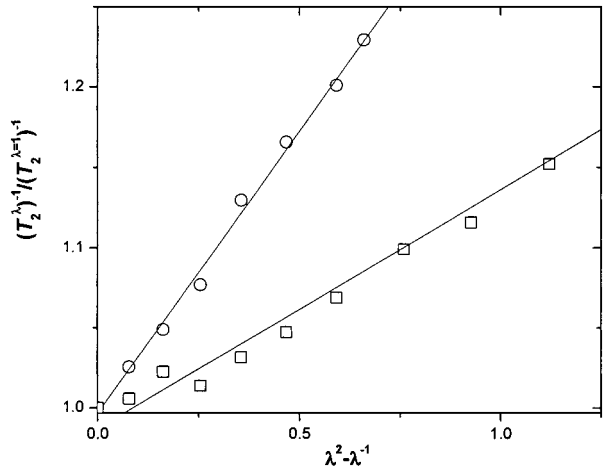

Figure 12. Normalized relaxation rate for the rubbery chains, $(T_2^{\lambda})^{-1}/(T_2^{\lambda=1})^{-1}$, against $\lambda^2 - \lambda^{-1}$ for *m*-PE (squares) and EPDM (circles). T_2 values for EPDM and the amorphous phase of *m*-PE were measured using the HEPS at 27 °C. Solid lines represent the results of a linear regression analysis of the data for *m*-PE [*intercept = 0.99 ± 0.01; slope = 0.15 ± 0.01; the correlation coefficient equals 0.992*] and for EPDM [*intercept = 1.00 ± 0.01; slope = 0.35 ± 0.01; the correlation coefficient equals 0.998*]. T_2 values for undeformed samples, $T_2^{\lambda=1}$, equal 270 ± 3 μs and 129 ± 2 μs for EPDM and *m*-PE, respectively (see Figure 9).

The results above suggest that physical network junctions, which originate from chain anchoring to crystals, would not be efficient in bearing the force and the applied force will be carried mainly by chemical cross-links and trapped chain entanglements. Thus,

larger strain-induced orientation in EPDM is apparently caused by a larger density of chemical cross-links in the sample compared to that of *m*-PE. Cured EPDM demonstrates good elastic recovery contrary to that of *m*-PE (see Figures 2 and 4). According to the T_2 experiments that were performed shortly after force release, T_2 values for the samples before and after deformation are the same, which suggests fast recovery of extended elastomeric chains to the random coil. However, it cannot be ruled out that a small residual chain elongation, which is not detected within the accuracy of the T_2 experiments, might still remain. Due to low density of chemical cross-links the retractive force in *m*-PE is rather small and elastic recovery of *m*-PE is hampered because of high density of physical network junctions, which were rearranged upon compression. It is mentioned in this respect that almost no elastic recovery is observed for un-cross-linked *m*-PE after compression force was removed. Heating of cross-linked *m*-PE above melting temperature causes almost complete elastic recovery after compression. It can be concluded that the density of chemical cross-links largely determines the elastic behavior of the samples studied.

4. Conclusions

It has been demonstrated that ^{1}H NMR T_2 relaxation experiments under uniaxial compression can provide useful information to help us to better understand the viscoelastic behavior of heterogeneous elastomeric materials, such as semicrystalline polymers, filled elastomers, thermoplastic elastomers, and thermoplastic vulcanizates. Strain-induced phase transitions and the orientation of viscoelastic chains under compression can be studied using this method. It should be mentioned that quantitative interpretation of the results is complicated by complex force distribution in the sample. The results of this study suggest that physical network junctions, which originate from chains anchoring to crystallites, would not be efficient in bearing the force and the applied force will be carried mainly by chemical cross-links and trapped chain entanglements. It appears that compression causes rearrangements of crystallites due to chain detachment from the crystal surface and its attachment to a neighboring crystal. An increase in the density of chemical cross-links is required for improvement of the elastic recovery of *m*-PE.

Acknowledgment. It is a pleasure to acknowledge Prof. J. P. Cohen-Addad, whose idea of solid-state NMR experiments under uniaxial compression was explored in the present study. Our gratitude also goes to J. F. Repin and F. A. M. op den Buijsch for their involvement in discussions and their provision of the samples. The author would like to thank the Technical Support Centre at DSM Research for construction of the compression unit.

References and Notes

(1) Treloar, L. R. G. *The Physics of Rubber Elasticity*, 3rd ed.; Clarendon Press: Oxford, England, 1975.
(2) Mark, J. E.; Erman, B. *Rubberlike Elasticity. A Molecular Primer*; John Wiley & Sons: New York, 1988.
(3) Nishio, T.; Chikarashi, T. *J. Macromol. Sci., Phys.* **1981**, *B19*, 445.
(4) Oikawa, H.; Murakami, K. *Polymer* **1982**, *23*, 1737.
(5) Fukumori, K.; Kurauchi, T.; Kamigaito, O. *J. Appl. Polym. Sci.* **1989**, *38*, 1313.
(6) Cohen-Addad, J. P.; Huchot, Ph.; Viallat, A. *Polym. Bull.* **1988**, *19*, 257.
(7) Cohen-Addad, J. P.; Huchot, P. *Macromolecules* **1991**, *24*, 6591.
(8) Cohen-Addad, J. P.; Soyez, E. *Macromolecules* **1992**, *25*, 6855.
(9) Kitamaru, R.; Horii, F.; Hyon, S.-H. *J. Polym. Sci., Polym. Phys. Ed.* **1977**, *15*, 821.
(10) Bergmann, K. *J. Polym. Sci., Polym. Phys. Ed.* **1978**, *16*, 1611.
(11) Fedotov, V. D.; Abdrashitiva, N. A. *Polym. Sci. USSR* **1980**, *A22*, 688.
(12) Ito, M.; Kanamoto, T.; Tanaka, K.; Porter, R. S. *Macromolecules* **1981**, *14*, 1779.
(13) Fedotov, V. D.; Abdrashitiva, N. A. *Polym. Sci. USSR* **1985**, *A27*, 287.
(14) Kakudate, T.; Kakizaki, M. Hideshima, T. *J. Polym. Sci., Polym. Phys. Ed.* **1985**, *23*, 787.
(15) Eckman, R. R.; Henrichs, P. M.; Peacock, A. J. *Macromolecules* **1997**, *30*, 2474.
(16) Choi, C.; Bailey, L.; Pintar, M. M. *J. Polym. Sci.: Part B: Polym. Phys.* **1997**, *35*, 2551.
(17) Hansen, E. W.; Kristiansen, P. E.; Pedersen, B. *J. Phys. Chem. B* **1998**, *102*, 5444; ibid. **1999**, *103*, 3552.
(18) Kitamaru, R.; Horii, F.; Zhu, Q.; Bassett, D. C.; Olley, R. H. *Polymer* **1994**, *35*, 1171.
(19) Hillebrand, L.; Schmidt, A.; Bolz, A.; Hess, M.; Veeman, W.; Meier, R. J.; van der Velden, G. *Macromolecules* **1998**, *31*, 5010.
(20) Kazuhiro, K.; Kaji, H.; Horii, F.; Bassett, D. C.; Olley, R. H. *Macromolecules* **1997**, *30*, 7516.
(21) Cheng, J.; Fone, M.; Reddy, V. N.; Schwartz, K. B.; Fisher, H. P.; Wunderlich, B. *J. Polym. Sci.: Part B: Polym. Phys.* **1994**, *32*, 2683.
(22) Morin, F. G.; Delmas, G.; Gilson, D. F. R. *Macromolecules* **1995**, *28*, 3248.
(23) Aharoni, S. M. *Macromolecules* **1983**, *16*, 1722.
(24) Gotlib, Yu. Ya.; Lifshits, M. I.; Shevelev, V. A.; Lishanskii, I. A.; Balanina, I. V. *Polym. Sci. USSR* **1976**, *18*, 2630.
(25) Fry, C. G.; Lind, A. C. *Macromolecules* **1988**, *21*, 1292.
(26) Litvinov, V. M.; Barendswaard, W.; van Duin, M. *Rubber Chem. Technol.* **1998**, *71*, 105 and references therein.
(27) Heymans, N. *Macromolecules* **2000**, *33*, 4226.
(28) Mathot, V. B. F.; Scherrenberg, R. L.; Pijpers, T. F. J.; Engelen, Y. M. T. In *New Trends in Polyolefin Science and Technology*; Hosoda, S., Ed.; Publisher Research Signpost: Trirandrum, India; 1996; p 71.
(29) Mathot, V. B. F.; Scherrenberg, R. L.; Pijpers, *Polymer* **1997**, *39*, 4541.
(30) Vanden Eynde, S.; Mathot, V. B. F.; Koch, M. H. J.; Reynaers, H. *Polymer* **2000**, *41*, 4889.
(31) McBrierty, V. J.; Douglass, D. C. *J. Polym. Sci.: Macromol. Rev.* **1981**, *16*, 295.
(32) Dujourdy, L.; Bazile, J. P.; Cohen-Addad, J. P. *Polym. Int.* **1999**, *48*, 558.
(33) Dikland, H. G. *Kautsch. Gummi Kunstst.* **1996**, *49*, 413.
(34) Ward, I. M.; Hadley, D. W. *An Introduction to the Mechanical Properties of Solid Polymers*; John Wiley & Sons: Chichester, England, 1993.
(35) Beansason, S.; Minick, J.; Moet, A.; Chum, S.; Hiltner, A.; Baer, E. *J. Polym. Sci., Part B: Polym. Phys.* **1996**, *34*, 1301.
(36) Bensason, S.; Stepanov, E. V.; Chum, S.; Hiltner, A.; Baer, E. *Macromolecules* **1997**, *30*, 2436.
(37) Chang, A. *Polym. Mater.: Sci. Eng.* **2001**, *84*, 354.
(38) Schmidt-Rohr, K.; Spiess, H. W. *Macromolecules* **1991**, *24*, 5288.
(39) Pérez, E.; VanderHart, D. L.; Crist, B.; Howard, P. R. Jr. *Macromolecules* **1987**, *20*, 78.
(40) Kuwabara, K.; Kaji, H.; Horii, F.; Bassett, D. C.; Olley, R. H. *Macromolecules* **1997**, *30*, 7516.
(41) Godovsky, Yu. K.; Bessonova, N. P. *Polym. Sci., Ser. A* **2001**, *43*, 880.

MA010208K